
A NOVEL DEEP PARALLEL TIME-SERIES RELATION NETWORK FOR FAULT DIAGNOSIS

Chun Yang

School of Automation Engineering, University of Electronic Science and Technology of China
Chengdu, Sichuan, China
beiluo@std.uestc.edu.cn

ABSTRACT

Considering the models that apply the contextual information of time-series data could improve the fault diagnosis performance, some neural network structures such as RNN, LSTM, and GRU were proposed to model the industrial process effectively. However, these models are restricted by their serial computation and hence cannot achieve high diagnostic efficiency. Also the parallel CNN is difficult to implement fault diagnosis in an efficient way because it requires larger convolution kernels or deep structure to achieve long-term feature extraction capabilities. Besides, BERT model applies absolute position embedding to introduce contextual information to the model, which would bring noise to the raw data and therefore cannot be applied to fault diagnosis directly. In order to address the above problems, a fault diagnosis model named deep parallel time-series relation network(*DPTRN*) has been proposed in this paper. There are mainly three advantages for *DPTRN*: (1) Our proposed time relationship unit is based on full multilayer perceptron(*MLP*) structure, therefore, *DPTRN* performs fault diagnosis in a parallel way and improves computing efficiency significantly. (2) By improving the absolute position embedding, our novel decoupling position embedding unit could be applied on the fault diagnosis directly and learn contextual information. (3) Our proposed *DPTRN* has obvious advantage in feature interpretability. Our model outperforms other methods on both TE and KDD-CUP99 datasets which confirms the effectiveness, efficiency and interpretability of the proposed *DPTRN* model.

Keywords Time-series fault diagnosis · Parallel computation · Time relationship unit · Decoupling position embedding unit

1 Introduction

With the rapid development of modern industry, industrial processes are becoming more and more miscellaneous and their internal structures are more complex. This requires the higher reliability and better maintainability about the components of the industrial process [1]. Therefore, the fault diagnosis techniques monitoring the industrial process conditions have attracted widespread attention [2].

Traditional model-based fault diagnosis methods are difficult to adapt to the growing modern industrial system, because the model-based methods need to pay attention to the internal mechanism of the industrial processes which make it very complicated. Therefore, data-driven methods have become a research hotspot [3]. The data-driven method analyzes the underlying laws of the data pattern according to the historical data collected in the industrial process, and generates a robust and accurate model.

Recently, a large number of scholars have proposed fault detection or fault diagnosis methods for various industrial processes. Xu et al. proposed a fault detection method combined with Principal Component Analysis (PCA), Independent Component Analysis (ICA) and Relevance Vector Machine (RVM) [4]. They considered the influence of the Gaussian and non-Gaussian components of the data comprehensively, and obtained relatively good experimental results. Our previous work used PCA and KPCA to perform fault detection on TE data [5, 6]. Wei et al. proposed a deep neural network named Deep Belief Network (DBN)-dropout to implement fault diagnosis [7]. Wang et al. designed a

network named extended deep belief network to fully exploit useful information in the raw data which achieved good performance on fault diagnosis [8]. The methods above handle the samples independently without considering the relationship between the samples. However, fault in industrial processes may change continuously and slowly over time because of the complicity of modern industry. In order to extract the features which represent the slow-changing characteristics, it is very necessary to utilize the characteristics of the time-series feature to model industrial processes over a period of time.

Compared with traditional machine learning methods, deep learning can avoid a lot of manual feature engineering work and automatically learn the potential high-dimensional expression of data, and has achieved a lot of practical results in the field of industrial fault detection and diagnosis [9]. Diego Cabrera et al. used Long-Short Term Memory (LSTM) to implement fault diagnosis on reciprocating compression machinery [10]. Zhang et al. applied the Bidirectional Recurrent Neural Network (BiRNN) to implement fault diagnosis on TE dataset [11]. Daria Lavrova et al. used the Gate Recurrent Unit (GRU) to analyze the time-series data and carry out anomaly detection [12]. In addition to the works mentioned above, there are a large number of scholars applying the RNN [13, 14, 15], LSTM [16, 17, 18, 19, 20], GRU [21, 22, 23] and Convolutional Neural Network (CNN) [24, 25, 26, 27] to solve the problem of fault diagnosis for time-series data.

However, the traditional network structure is either a serial calculation method such as RNN, or requires a deeper network structure or larger convolution kernels such as CNN to extract long-term evolution features of the industrial process. This makes them inefficient when performing fault diagnosis. Therefore, the traditional neural network cannot meet the increasing requirements for real-time fault diagnosis. Because of the high efficiency of MLP and its parallel computing characteristics, the deep learning network structure which adopts the full MLP structure has received the attention of scholars in the field of computer vision (CV) and natural language processing (NLP) [28, 29, 30]. Besides, a Bidirectional Encoder Representation from Transformers (BERT) model including an absolute position embedding was proposed to introduce contextual information of time-series data for performance improvement in the field of NLP. However, the absolute position embedding cannot be directly applied to improve the fault diagnosis performance because it will bring noise to the raw data.

Inspired by the research above, this paper proposed a fault diagnosis method named deep parallel time-series relation network (DPTRN) which is composed of three parts, including time relationship unit, decoupling position embedding unit and classification layer.

Different from the traditional neural network structure mentioned above, our proposed time relationship unit is constructed through a MLP structure with shared weight. It can exploit all time nodes of a time-series sample in a parallel way and does not require deep structure or huge parameter amount, which indicates that the feature extraction efficiency of the DPTRN is greatly improved. Considering that the time relationship unit cannot extract the contextual feature of the industrial process data and the absolute position embedding cannot be applied to fault diagnosis directly, we proposed a decoupling position embedding unit in the framework which considers the contextual information of the time-series data.

By combining the calculation results of time relationship unit and decoupling position embedding unit with the features of each time node, a comprehensive historical information vector that integrates evolution information of the time-series data will be obtained, and it will be input into the classification layer together with the features of current time node. The superiority of the proposed model is validated on the TE dataset and KDD-CUP99 dataset.

The main contributions of this paper are summarized as follows.

- Inspired by MLP's renewed attention in various fields, the time relationship unit was proposed to extract the relationship between each historical time node and the current time node in a parallel way, which could indicate the importance of each historical time node for fault diagnosis. While ensuring the feature extraction capability of the model, the computational efficiency of fault diagnosis is greatly improved.
- In order to make full use of the contextual information of the time-series data, we proposed a novel unit, named decoupling position embedding unit, in the diagnosis framework, which would achieve significant improvement for the fault diagnosis in the industrial process.
- Our proposed DPTRN model provides a convenient way to interpret the output of the framework. For the time relationship unit, its output could explain the importance of each historical time node for fault diagnosis, and the output of decoupling position embedding unit could explain the relationship of the importance of historical information over time. Compared with traditional deep learning networks that use hidden state vectors to express evolutionary characteristics and therefore does not reflect any physical meaning, DPTRN is good at feature interpretability.

The rest of this paper is organized as follows. Section 2 briefly introduces the theoretical background including multilayer perceptron and batch normalization. Section 3 details the pipeline used for fault diagnosis and the proposed DPTRN. In Section 4, the fault diagnosis and fault detection cases of the TE dataset and KDD-CUP99 dataset verify the high efficiency, effectiveness and interpretability of the proposed method. Finally, conclusions are drawn in Section 5.

2 Theoretical background

2.1 Multilayer perceptron

The MLP is a neural network structure that feeds forward the input data [31]. MLP has multiple layers, including input, hidden, and output layers with neurons between each layer are fully connected. The number of neurons in the input layer is consistent with the input data, the number of hidden layers is a hyperparameter, and the number of neurons in the output layer is determined according to the task. The output of each neuron is the result of the activation function, and the input of the activation function is the weighting operation of the input of the neuron connection [32]. Consider the input as X , the output of layer l in MLP is:

$$o^l = \sigma(w^l X + b^l) \quad (1)$$

Where matrix w^l and b^l represent the corresponding network weight and bias respectively. Function $\sigma(\bullet)$ is the non-linear activation function of the layer which is optional in Sigmoid, tanh, Relu et al. The output of layer l will be used as the input of layer $l + 1$. The w and b of each layer in MLP approximate the optimal solution by calculating the loss of the cross entropy function through supervised learning. Cross entropy loss can minimize the difference between model output and expected output:

$$L = - \sum_{i=1}^K y_i \log(p_i) \quad (2)$$

Where K is the total number of categories, y_i is the corresponding label (when considering the i -th category, y_i is 1, otherwise it is 0), p_i is the output of neural network.

2.2 Batch normalization

As the deep neural network is difficult to train due to the internal covariate shift, the method proposed in this paper used the batch normalization layer. Batch normalization can perform standardization for each batch, allowing the model to use a higher learning rate in training, reducing the training steps and the training difficulty of the method [33]. For the input $X = (x_1, x_2 \dots, x_n)$ with n dimension, batch normalization layer normalizes the data in the following way:

$$\hat{x}_i = \frac{x_i - \mu_B}{\sqrt{\text{Var}[x_i]}} \quad (3)$$

Where μ_B , $\text{Var}[x_i]$ are mean value and standard deviation of the corresponding batch respectively. For \hat{x}_i after simple normalization, Batch normalization also introduced parameters γ_i and β_i to scale and move the normalized value, so that the representation between each layer is not affected by the parameters of each layer.

$$f_i = \gamma_i \hat{x}_i + \beta_i \quad (4)$$

Where γ_i and β_i are learnable parameters. Due to space limitations, this paper does not give more introduction of batch normalization. For more principles and training details of batch normalization, please refer to [33].

Here we apply the batch normalization immediately before the activation layers of MLPs, because it can accelerate the convergence of the DPTRN end-to-end training process and improve the robustness of the method. In addition, the activation function $f(\bullet)$ we applied is Relu, and its combined utilization with batch normalization can further solve the problem of deep network gradient disappearance. So, it is a natural choice to apply batch normalization in the DPTRN model.

3 Framework of the DPTRN

This section introduces the DPTRN method for fault diagnosis of time-series data in detail. The framework and illustration of the proposed method are shown in Figure 1. Specifically, the procedure of fault diagnosis can be described as follows:

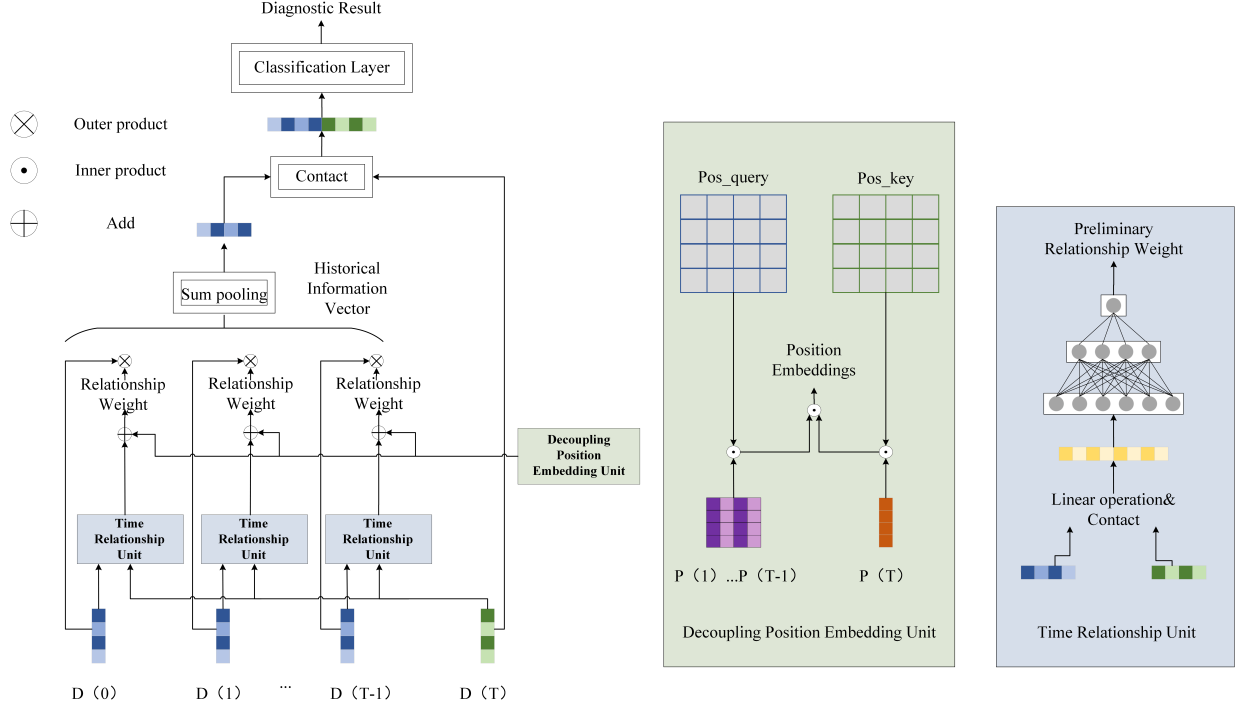


Figure 1: The structure of DPTRN, the left part includes the overall structure and illustration of proposed DPTRN, the middle part is the decoupling position embedding unit in detail, and the right part is the detailed structure of the time relationship unit.

- Establish time-series data training set $X = (x_1, x_2 \dots, x_n) \in R^{N \times T \times M}$. Where N , T and M mean the number of samples, length of time-series, feature dimensions respectively. $x_i \in R^{T \times M}$ is the i th sample of the training set.
- For sample x_i , divide the sample into current time node $D(T) \in R^M$ (The green vector in Figure 1) and historical time node $D(k) \in R^M, k = 0, 1 \dots, T - 1$ (The blue vector in Figure 1).
- For each historical time node $D(k)$, it will be input to the time relationship unit together with the current time node $D(T)$ to get preliminary relationship weight which is a scalar. Details about time relationship unit will be introduced in section 3.1.
- For each historical time node K and current time node T , DPTRN firstly generates absolute position embeddings (respectively the purple vector and brown vector in Figure 1), and then uses the position query matrix (The blue matrix in Figure 1) and the position key matrix (The green matrix in Figure 1) to perform multiple mappings, and finally generates decoupling position embeddings which are scalar too. Regarding the decoupling position embedding unit the details will be introduced in section 3.2.
- Add the output of the time relationship unit and the decoupling position embedding unit to get the time relationship weight corresponding to each historical time node. A comprehensive historical information vector can be obtained by weighting and sum pooling the features of corresponding historical time nodes and time relationship weights.
- Finally, the historical information vector will be contacted with the features of the current time node and input to the classification layer to obtain the fault diagnosis result. The details of the classification layer will be explained in section 3.3.

3.1 Time relationship unit

The detailed structure of the time relationship unit is shown in the right part of Figure 1. The purpose of designing the time relationship unit is to analyze the relation between each historical time node and the current time node of the time-series data, that is, the importance of each historical time node for diagnosing the current sample. We expect to be able to weaken the impact of time nodes that are not important to diagnosis through the output of the time relationship

unit, and on the other hand, it can also enhance the impact of time nodes that are useful for diagnosis. The specific implementation of the time relationship unit is a deep MLP network. Therefore, the unit can perform long-term feature interaction in a parallel way, which greatly improves the computational efficiency.

As shown in the figure, the features of the historical time node and the current time node will be linearly operated and contacted before being input to the MLP. The purpose of linear operation is to improve the discrimination between the features of the historical time node and the current time node, thereby enhancing the expressive ability of the time relationship unit. The DPTRN proposed in this paper used addition and subtraction as linear operations because of their high efficiency and good performance. The vector that will be input to the MLP in the time relationship unit is:

$$V_K = [D(T), D(K), D(T) - D(K), D(T) + D(k)] \quad (5)$$

Where the dimension of V_K is $4M$. Then utilize the MLP output the preliminary relationship weight. In this paper, the number of MLP layers in the time relationship unit is set to be 3, which can ensure the model's high computational efficiency while guaranteeing the model's characterization capability. The output of the time relationship unit is:

$$RW_{pre_K} = W_3 \sigma (W_2 (\sigma (W_1 V_K + b_1)) + b_2) + b_3 \quad (6)$$

Where RW_{pre_K} represents the preliminary relationship weight of the corresponding historical time node K , matrix W and b represent the corresponding network weight and bias of each layer respectively. The activation function $\sigma(\bullet)$ we applied is Relu.

It is worth noting that because the time relationship unit does not consider the context of each historical time node, so that RW_{pre} is only the preliminary relationship weight. In addition, the time relationship unit shares the weight for all historical time nodes, which greatly reduces the model size of DPTRN and the difficulty of model training. Besides, in order to highlight the importance of specific historical time node and prevent important historical nodes from being smoothed, the time relationship unit will not perform *softmax* normalization on the final RW_{pre} , which means that the sum of RW_{pre} at each historical time node is not 1. The time relation unit interacts features of each time node of the time-series data in a novel structure, which improves the diagnostic efficiency of the model significantly.

3.2 Decoupling position embedding unit

The detailed structure of the decoupling position embedding unit is shown in the green part of Figure 1. The design of the decoupling position embedding unit was inspired by the introduction of absolute position embedding when the BERT model which in the NLP field processed the text sequence data [34]. However, absolute position embedding cannot be applied to the field of fault diagnosis directly, because it will bring noise to the raw data. Our proposed decoupling position embedding unit is able to take into account the contextual information of time-series data without interfering with the raw features in a novel way. Because the decoupling position embedding unit is an auxiliary part of the time relationship unit, and we don't want use too many parameters for this unit, so we adopt the matrix mapping method to achieve it.

For each time node in the time-series data, an absolute position embedding will first be generated:

$$\begin{cases} PE_{(pos,2i)} = \sin \left(pos/10000^{2i/d_{\text{model}}} \right) \\ PE_{(pos,2i+1)} = \cos \left(pos/10000^{2i/d_{\text{model}}} \right) \end{cases} \quad (7)$$

Where pos means the position of time node K in time-series data, d_{model} is the constant T which represents the length of the time-series sample. Absolute position embedding performs sin or cos transformation according to the position of each time node in the time-series data sample.

In BERT, the absolute position embeddings were directly added to the raw features, and it was expected that the model can learn the context through those embeddings. Assuming that this paper had adopted the same method of introducing absolute position embedding as BERT, that is, position embedding without decoupling, then the model structure shown in Figure 2 will be obtained.

It is worth noting that the features used in BERT were obtained through embedding layer mapping which were trainable, and could cooperate with absolute position embedding during the training process. However, in the field of fault diagnosis, the features are generally collected in the industrial process which are not trainable. This means that directly adding the absolute position embedding to the raw data may change the physical meaning of each channel in the feature vector, thereby reducing the model reliability and effectiveness. In order to illustrate the negative effects of absolute position coding fully, we conducted an ablation experiment in section 4.5.

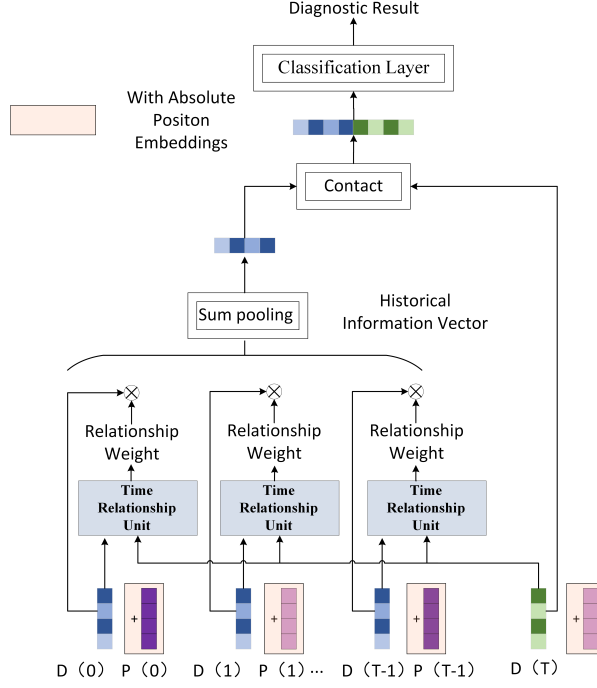


Figure 2: The structure of the $DPTRN_b$ model which uses absolute position embedding instead of decoupling position embedding. $DPTRN_b$ directly adds the absolute position embeddings to the raw features

The purpose of designing the decoupling position embedding unit in $DPTRN$ is to guide the model to learn contextual information of time-series data without introducing noise into the raw data. For any historical time node K , its decoupling position embedding is calculated as follows:

$$DPE_K = (PE_K \odot P_{query}) \odot (PE_T \odot P_{key}) \quad (8)$$

Where PE_K and PE_T indicate the absolute position embeddings corresponding to time node K and current time node T respectively. P_{query} and P_{key} represent the mapping matrix corresponding to the historical time node and the current time node respectively, that is, the blue and green matrix in Figure 1. In order to reduce the computational complexity, the dimension of the mapping matrix is set to a square matrix of $M \times M$. DPE_K is a scalar, which represents the positional relationship of the current time node K in the time-series data.

Add the decoupling position embedding DPE_K and the preliminary relationship weight RW_{pre_K} which is obtained from the time relationship unit to get the final relationship weight corresponding to historical time node K :

$$RW_K = RW_{pre_K} + DPE_K \quad (9)$$

For all historical time nodes, a relationship weight vector can be obtained:

$$RW = \frac{[RW_1, RW_2, \dots, RW_{T-1}]}{\sqrt{M}} \quad (10)$$

Where the \sqrt{M} is the regularization coefficient which is beneficial for model parameter optimization. The comprehensive historical information vector can be obtained by taking the outer product of the relationship weight vector and the original feature data of each historical node and summing them one by one:

$$HI = \text{sumpooling}(RW \otimes X_{T-1}) \quad (11)$$

Where X_{T-1} represents samples in the time-series data except the current time node sample. Except sum pooling, it can also use contacting, average pooling or other pool methods to obtain the comprehensive historical information

Table 1: The Description of the two datasets used for validation

dataset	dim	length	training	valid	testing
TE	52	100	58543	3082	10875
KDD-CUP99	39	100	72000	8000	20000

vector. In this paper, the sum pooling layer is adopted for the considerations of computational efficiency, and other pooling operations are left for follow-up research.

Then contacting the historical information vector HI with the original features of the current time node to obtain the vector that will be input to the classification layer:

$$I = [HI, D(T)] \quad (12)$$

We believe that historical information and current node information should have the same importance, so that the vector I not only contains the information of the historical node, but also considers the information of the current node.

3.3 Classification layer

The vector I will be input to the classification layer to obtain the final fault diagnosis result. The classification layer is also a three-layer MLP structure. The output of the classification layer is calculated as follows:

$$\hat{y} = \text{softmax}(W'_3 \sigma(W'_2 (\sigma(W'_1 I + b'_1)) + b'_2) + b'_3) \quad (13)$$

Where matrix W' and b' represent the corresponding network weight and bias of each layer respectively. The activation function $\sigma(\bullet)$ is Relu.

The fault diagnosis result can be obtained according to the output result of the classification layer.

3.4 Training strategy & Online Diagnosis

The DPTRN fault diagnosis model proposed in this paper adopted the deep structure of full MLP to implement long-term feature interaction, and batch normalization was used between MLP layers to reduce the difficulty of model training. In addition, in order to avoid over-fitting of the model, this paper also applied L2 regularization and dropout strategies.

In online fault diagnosis, the detected data is also required to be arranged in the same time-series data format as the training dataset, and the data will be input into the model according to the same data pipeline as training dataset to obtain the corresponding fault detection results.

4 Experiment

In order to verify the effectiveness of the model proposed in this paper, an industrial process fault diagnosis dataset named Tennessee Eastman (*TE*) and a network attack anomaly detection dataset named KDD-CUP99 are used for comparative experiments. The evaluation indicators used in the comparative experiment include, recall rate, accuracy rate, F1 value, model size and floating point operations (*FLOPS*).

4.1 Datasets

The details of the two time-series datasets used for the performance comparison described as follows.

- Tennessee-Eastman chemical process, which simulated a real chemical production process. It has been widely used as a benchmark process to evaluate fault detection and fault diagnosis methods. This process includes one normal state and 20 fault states. TE process flow chart is shown in Figure 3. The details about the TE process can be found in [35].
- KDD-CUP99, which recorded 7 million network traffic connection records within 7 weeks. The network traffic data were labeled as normal or attacked data. More details about the data can be found in [36].

The main information about the two datasets used in this paper is shown in Table 1, including the feature dimensions, the length of the time series, the number of samples in the training set, validation set and the test set.

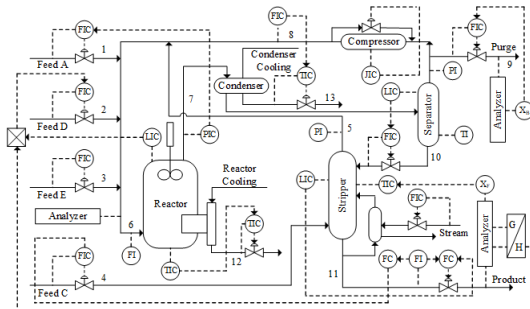


Figure 3: The flowchart of the Tennessee Eastman process.

Table 2: The network structure of the methods used for comparison.

Model	Structure
MLP	$\text{View}(x) \rightarrow \text{MLP}(256, 128, 64) \rightarrow \text{softmax}$
LSTM+MLP	$\text{LSTM}(\text{layer}=2, \text{hidden}=128) \rightarrow \text{LSTM}(\text{layer}=2, \text{hidden}=64) \rightarrow \text{MLP}(256, 128, 64) \rightarrow \text{softmax}$
BiLSTM+MLP	$\text{LSTM}(\text{layer}=2, \text{hidden}=128) \rightarrow \text{LSTM}(\text{layer}=2, \text{hidden}=64) \rightarrow \text{MLP}(256, 128, 64) \rightarrow \text{softmax}$
1DCNN+MLP	$1\text{DCNN}(\text{out_channels}=256, \text{filter}=5*5) \rightarrow 1\text{DCNN}(\text{out_channels}=512, \text{filter}=7*7) \rightarrow 1\text{DCNN}(\text{out_channels}=256, \text{filter}=11*11) \rightarrow \text{MLP}(256, 128, 64) \rightarrow \text{softmax}$

They all use the same classification layer $\text{MLP}(256, 128, 64)$.

It should be noted that in order to avoid information leakage when processing datasets, this paper applies data non-crossover instead of sliding windows to collect time-series data. This means that each time node data in the dataset would only belongs to training samples or test samples. To allow fair comparison, we employ the same data preprocessing for all methods.

4.2 Models for comparison

The proposed method is compared with the pure MLP, LSTM, BiLSTM and IDCNN to verify validity and efficiency. Since the core innovation of this paper is the proposed time relationship unit and decoupling position embedding unit that can be regarded as a new feature extractor, for fairness, the same classification layer is applied when comparing the performance among the those methods.

The network structures of the above-mentioned method for comparison are shown in Table 2.

In addition, in order to illustrate the effects of the time relationship unit and the decoupling position embedding unit separately, DPTRN_a and DPTRN_b are introduced in the performance comparison. For DPTRN_a , it does not use position embedding unit but only use the time relationship unit (that is, directly uses the preliminary relationship weight in the formula 6 as the final relationship weight). For DPTRN_b , it is the model in shown Figure 2, that only uses absolute position embedding instead of using decoupling position embedding unit. In order to distinguish, the model proposed in this paper is called DPTRN in the comparison. The structure of the MLP in the time relationship unit in DPTRN is (512, 128).

4.3 Implementation details

To keep it fair, all the compared models mentioned in this paper are trained and inferred on the same experimental platform (RTX 2080ti with 12G memory). Batch size of each network is set to be 32, epoch is 60, and learning rate is $6e^{-4}$. The L2 regularization coefficient is 0.0001.

4.4 Case study

In order to verify the effectiveness of the proposed DPTRN method, the performances on the KDDCUP99 dataset (fault detection) and TE dataset (fault diagnosis) are compared with the various baseline methods mentioned above. The detailed comparison results are shown in the table 3 and the best part of the comparison results are bolded. In addition, we also compared the model size and the floating point operations of DPTRN with various baseline methods to verify the efficiency of the proposed method, and the results are shown in the table 4.

Table 3: The fault diagnosis results of various methods on the KDD-CUP99 dataset and TE dataset.

Method	KDD-CUP99 dataset			TE dataset		
	Recall(%)	Accuracy (%)	F1(%)	Recall(%)	Accuracy (%)	F1(%)
MLP	0.9785(0.9762)	0.9785(0.9762)	0.9785(0.9762)	0.9520(0.9434)	0.9667(0.9650)	0.9559(0.9468)
LSTM+MLP	0.9835(0.9830)	0.9836(0.9829)	0.9835(0.9829)	0.9635(0.9226)	0.9636(0.9180)	0.9635(0.9128)
BiLSTM+MLP	0.9838(0.9830)	0.9838(0.9830)	0.9838(0.9830)	0.9889(0.9338)	0.9895(0.9208)	0.9892(0.9218)
1DCNN+MLP	0.9866(0.9826)	0.9867(0.9826)	0.9966(0.9825)	0.9898(0.9889)	0.9904(0.9890)	0.9901(0.9890)
DPTRN	0.9881(0.9870)	0.9881(0.9870)	0.9881(0.9870)	0.9960(0.9943)	0.9963(0.9948)	0.9961(0.9944)

All models were trained on the same training set. Recall, accuracy, and F1 were all obtained on the same test set. The results outside the brackets are the best experimental results of 5 different random seeds. The results inside the brackets are the average result of 5 experiments.

4.4.1 The effectiveness of different methods

The models used for effectiveness comparison include MLP, LSTM+MLP, BiLSTM+MLP, 1DCNN+MLP and our proposed DPTRN.

It can be seen from the table 3 that the experimental performance of the simple MLP model is the worst. It is reasonable that it has a simple structure and does not have the ability to process a large number of features of the time-series data. Contrastively, both LSTM + MLP and BiLSTM + MLP have achieved better fault detection or fault diagnosis results than simple MLP. It is because that LSTM can uses a recurring unit with shared weights to extract potential features and generate a hidden state vector to represent time evolution characteristics through serial calculation. 1DCNN also achieves satisfactory fault diagnosis performance because 1DCNN uses different size convolution kernels to interact features between different time nodes in time-series data.

Compared with various baseline methods, DPTRN achieves the best experimental results. It is because that the time relationship unit has powerful feature extraction capability on time-series data and the Decoupling position embedding unit can effectively synthesize the information of various time nodes, which indicates that our proposed DPTRN has the ability to extract discriminating features on time-series data effectively in a novel way.

4.4.2 The efficiency of different methods

Table 4: The efficiency of various methods on the TE dataset.

Method	Model size	FLOPs
MLP	2995K	1.37M
LSTM+MLP	368K	31.19M
BiLSTM+MLP	368K	85.27M
1DCNN+MLP	4679K	91.88M
DPTRN	252K	34.55M

To investigate the model efficiency, the model sizes and FLOPs of different methods are listed in Table 4.

It can be that the simple MLP model has the biggest model size. This method uses the classification layer immediately after flattening the time-series data which makes the input vector dimension extremely large and increases the number of parameters greatly. But at the same time, due to the simple structure of the simple MLP, its FLOPs is low, and the fault diagnosis task can be completed with higher efficiency. Since the recurrent units in LSTM share weights, the model size is greatly reduced, which reduces the difficulty of training. For LSTM, it is limited by its complex serial calculation design, therefore, the FLOPs of both LSTM + MLP and BiLSTM + MLP have been significantly improved, which reduces their calculation efficiency. 1DCNN needs to use different convolution kernel sizes or deep structure to realize long-term feature interaction, which increases the model size and training difficulty of CNN. In addition, the complex convolution operation of CNN will increase its FLOPs, making 1DCNN also unable to meet the requirement of real-time fault detection or fault diagnosis.

Our proposed DPTRN can extract features in parallel, which makes it more computationally efficient. As shown in table 4, the DPTRN has obvious advantages in model size, which makes training DPTR easier. Besides, DPTRN has

lowest FLOPs, this means the proposed method can meet the increasing need for high efficiency in industrial processes. This also verifies the effectiveness of parallel computing emphasized in this paper.

Based on the results on the above two datasets, it can be seen that the DPTRN method proposed in this paper has the advantage of high computational efficiency due to its parallel computing characteristics. In addition, it has less parameter numbers and is easier to train model because its time relationship unit shares weights and the model can be summed up as a 6-layer MLP structure. Furthermore, the DPTRN model achieves the best fault diagnosis and fault detection results, which further proves the effectiveness, rationality and robustness of the time relationship unit and decoupling position embedding unit proposed in this paper. Therefore, our proposed DPTRN can realize efficient and reliable fault diagnosis and has the potentiality to meet the real-time fault detection or fault diagnosis requirement in the industrial process.

4.5 Ablation study

Table 5: The ablation experiment results of DPTRN

Method	KDD-CUP100 dataset			TE dataset		
	Recall(%)	Accuracy (%)	F2(%)	Recall(%)	Accuracy (%)	F2(%)
DPTRN _a	0.9813(0.9785)	0.9813(0.9807)	0.9813(0.9791)	0.9825(0.9795)	0.9858(0.9839)	0.983(0.9805)
DPTRN _b	0.9752(0.9713)	0.9752(0.9758)	0.9752(0.9723)	0.9741(0.9314)	0.9800(0.9590)	0.9754(0.9340)
DPTRN	0.9881(0.9870)	0.9881(0.9870)	0.9881(0.9870)	0.9960(0.9943)	0.9963(0.9948)	0.9961(0.9944)

DPTRN_a does not use position embedding unit but only use the time relationship unit. DPTRN_b is the model that only uses absolute position embedding instead of using decoupling position embedding unit.

In order to further verify the validity and rationality of the proposed time relationship unit separately and the decoupling position embedding unit. we conducted ablation experiments for these two units. The experimental results are shown in the table 5

It could be seen that all of the metrics of DPTRN_a on both of the two datasets are around 98%, which surpasses simple MLP and LSTM. Therefore, the time relationship unit could extract the characteristics of time-series data better.

For the model of DPTRN_b, it’s performance metrics are not so satisfying, and even worse than that of simple MLP on the TE dataset. It is consistent with the hypothesis, that the absolute position embedding cannot be directly applied to the field of fault diagnosis because it would bring noise to the raw data.

Our proposed DPTRN model has a significant improvement compared with the results based on DPTRN_a and DPTRN_b, which further verifies the advantages our the framework effectiveness of the decoupling position embedding unit proposed in this paper.

Based on the results of the above ablation experiments, it can be seen that the time relationship unit can effectively extract the evolution features of the time-series data, the decoupling position embedding unit proposed in this paper can further improve the performance of the model.

4.6 The interpretability of DPTRN

The proposed framework combined with the time relationship unit and the decoupling position embedding unit could significantly improve the performance, and it is quite interesting to investigate how the two units affect the results. Therefore, we randomly selected two fault samples from the TE dataset and compared them with normal samples to check the output of the two units, and analyze the internal working principles of these two units.

4.6.1 The interpretability of time relationship unit

For the time relationship unit, the outputs of the two fault samples mentioned above are shown in the Figure 4. In the heatmap of each subgraph, The redder cubes indicate that the current time nodes have a higher preliminary relationship weight, and the bluer cubes are conversely. For the left subgraph, it can be seen that the outputs with larger weights are with dark red. By integrating with the right subgraph, one could see that the red parts just map to the features that indicate the significant difference between the fault sample and normal sample. The corresponding parts for the two subgraphs are marked with black box and these marked time nodes contain long-term evolutionary information that is useful for correct fault diagnosis.

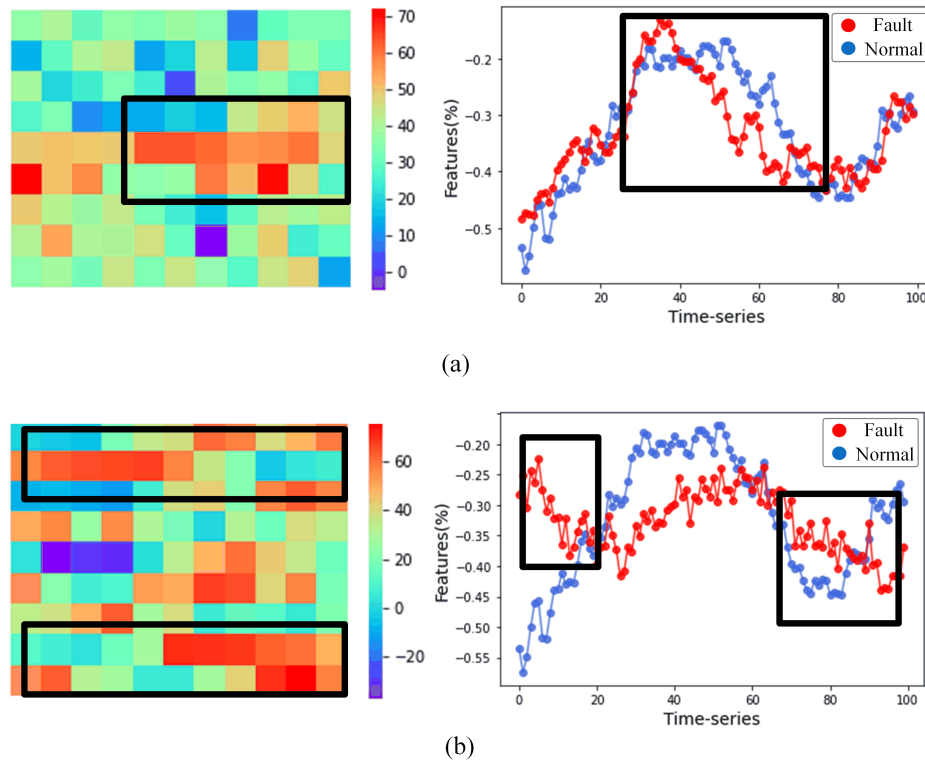


Figure 4: The heatmap output of the time relationship unit and the corresponding feature representation for TE dataset. (a) and (b) show the results for the two fault samples respectively. There are 2 subgraphs in the figure. The left half part of each subgraph is the heatmap output, which represents the preliminary relationship weight output of time relationship unit. Each block represents a time node from 0 to $T-1$, and the figure is arranged from left to right and from top to bottom. And the right half part is the feature of each time node. The blue curve indicates the normal sample, the red curve indicates the fault sample. The data masked with black box indicates the part showing significant difference between normal and fault samples.

In addition, it is worth noting that the time relationship unit outputs a completely different preliminary relation weights for the two types of fault samples. For each sample, historical time nodes that contain important information for fault diagnosis may be distributed anywhere in the length of the time series, which requires time relationship unit can output the correct weight at each time node. By using the different weights to extract the evolution information in the time-series data, subsequent classification layer can more easily focus on these historical nodes that are beneficial to fault diagnosis, which greatly improves the performance of fault diagnosis.

4.6.2 The interpretability of decoupling position embedding unit

For the decoupling position embedding unit, since its input is the absolute position embedding determined by the timing length, the outputs of each sample are the same and shown in Figure 5. Once can see that the weight outputs of the decoupling position embedding unit become larger as the historical time node gets closer and closer to the current time node. Therefore, for the decoupling position embedding unit, the closer the distance to the current time node, the more valuable the time nodes are.

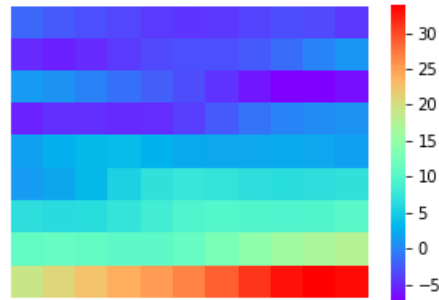


Figure 5: The weight output of the decoupling position embedding unit in TE dataset. According to the time node from 0 to T-1, the figure is arranged from left to right and from top to bottom.

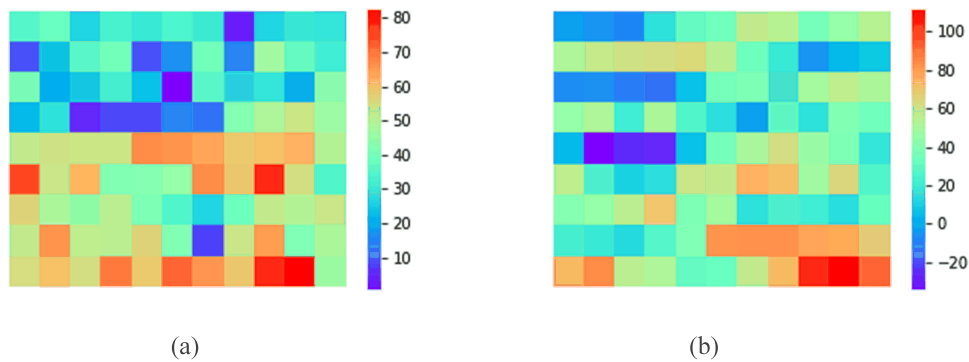


Figure 6: The relationship weight heatmaps of the two fault samples output from the combination of the two units. According to the time node from 0 to T-1, the figure is arranged from left to right and from top to bottom. The redder cubes indicate that the current time nodes have a higher preliminary relationship weight, and the bluer cubes are conversely.

It is worth noting that the outputs of the decoupling position embedding unit are learnable, which means that it has learned results that are consistent with human prior knowledge, that is, the reference value of information about a long time ago will decrease.

4.6.3 The interpretability of relationship weight

For the two random time series fault samples mentioned above, the final outputs by combining the time relationship unit and the decoupling position embedding unit are shown in Figure 6. As shown in the figure, the final relationship weights become smoother, and have the ability to indicate both the importance of each historical time node and the relative importance of the times nodes among the time series for fault diagnosis.

For the neural network structures, such as RNN, LSTM and GRU, they use a hidden state vector to represent the features of the evolution of the time-series data, which cannot explain the specific physical meaning. For CNN, it applies the convolution kernel to complete the feature interaction of time-series data, and is also difficult to explain the specific physical meaning of the convolution kernel. For our proposed DPTRN, the time relationship unit explains the importance of each historical time node for fault diagnosis, and the decoupling position embedding unit explains the relationship of the importance of historical information over time.

Therefore, the proposed DPTRN are more interpretable than the traditional deep neural network.

5 Conclusion

In this article, a deep parallel time-series relation network model for fault diagnosis of time-series data is proposed. Considering that traditional deep learning networks are limited to parallel computing when analyzing time-series data, the DPTRN model proposed in this paper uses serial time relationship units to extract evolutionary features and improve computational efficiency. In order to introduce the contextual information of time-series data to the model, the decoupling position embedding unit is introduced to DPTRN.

Fault diagnosis and fault detection experiments were carried out on TE and KDD-CUP99 datasets respectively. Experimental results show that the proposed DPTRN model has better effectiveness, robustness and computational efficiency. In addition, the output of the time relation unit and the decoupling position embedding unit is analyzed in detail, and the results show the reliability and stronger interpretability of DPTRN.

When dealing with time-series data, this paper refocuses attention on MLP and proves the feasibility and effectiveness of parallel computing. This provides a new idea for solving the problem of time-series data fault diagnosis. In this paper, only the original features are used for historical time nodes, and further research on how to make full use of historical data will be an interesting direction.

References

- [1] Te Han, Chao Liu, Wenguang Yang, and Dongxiang Jiang. Deep transfer network with joint distribution adaptation: A new intelligent fault diagnosis framework for industry application. *ISA transactions*, 97:269–281, 2020.
- [2] Yaguo Lei, Bin Yang, Xinwei Jiang, Feng Jia, Naipeng Li, and Asoke K Nandi. Applications of machine learning to machine fault diagnosis: A review and roadmap. *Mechanical Systems and Signal Processing*, 138:106587, 2020.
- [3] Shen Yin, Xianwei Li, Huijun Gao, and Okyay Kaynak. Data-based techniques focused on modern industry: An overview. *IEEE Transactions on Industrial Electronics*, 62(1):657–667, 2014.
- [4] Yuan Xu, Sheng-Qi Shen, Yan-Lin He, and Qun-Xiong Zhu. A novel hybrid method integrating ica-pca with relevant vector machine for multivariate process monitoring. *IEEE Transactions on Control Systems Technology*, 27(4):1780–1787, 2018.
- [5] Jian Zhang, Jianxiao Zou, Jiyang Zhang, Qian Tao, Xingtai Gui, Hongbing Xu, and Shicai Fan. A novel deep dpca-svm method for fault detection in industrial processes. In *2019 IEEE 58th Conference on Decision and Control (CDC)*, pages 2916–2921. IEEE, 2019.
- [6] Chun Yang, Lujing Tao, Jian Zhang, Xingtai Gui, Jiyang Zhang, Jianxiao Zou, and Shicai Fan. A fault detection method based on the deep extended pca-svm in industrial processes. In *2021 American Control Conference (ACC)*, pages 3620–3625. IEEE, 2021.
- [7] Yuqin Wei and Zhengxin Weng. Research on te process fault diagnosis method based on dbn and dropout. *The Canadian Journal of Chemical Engineering*, 98(6):1293–1306, 2020.
- [8] Yalin Wang, Zhuofu Pan, Xiaofeng Yuan, Chunhua Yang, and Weihua Gui. A novel deep learning based fault diagnosis approach for chemical process with extended deep belief network. *ISA transactions*, 96:457–467, 2020.
- [9] Duy-Tang Hoang and Hee-Jun Kang. A survey on deep learning based bearing fault diagnosis. *Neurocomputing*, 335:327–335, 2019.
- [10] Diego Cabrera, Adriana Guamán, Shaohui Zhang, Mariela Cerrada, Rene-Vinicio Sanchez, Juan Cevallos, Jianyu Long, and Chuan Li. Bayesian approach and time series dimensionality reduction to lstm-based model-building for fault diagnosis of a reciprocating compressor. *Neurocomputing*, 380:51–66, 2020.
- [11] Shuyuan Zhang, Kexin Bi, and Tong Qiu. Bidirectional recurrent neural network-based chemical process fault diagnosis. *Industrial & Engineering Chemistry Research*, 59(2):824–834, 2019.
- [12] Daria Lavrova, Dmitry Zegzhda, and Anastasiia Yarmak. Using gru neural network for cyber-attack detection in automated process control systems. In *2019 IEEE International Black Sea Conference on Communications and Networking (BlackSeaCom)*, pages 1–3. IEEE, 2019.
- [13] Ya Su, Youjian Zhao, Chenhao Niu, Rong Liu, Wei Sun, and Dan Pei. Robust anomaly detection for multivariate time series through stochastic recurrent neural network. In *Proceedings of the 25th ACM SIGKDD International Conference on Knowledge Discovery & Data Mining*, pages 2828–2837, 2019.
- [14] Pavel Filonov, Fedor Kitashov, and Andrey Lavrentyev. Rnn-based early cyber-attack detection for the tennessee eastman process. *arXiv preprint arXiv:1709.02232*, 2017.

- [15] Mikel Canizo, Isaac Triguero, Angel Conde, and Enrique Onieva. Multi-head cnn-rnn for multi-time series anomaly detection: An industrial case study. *Neurocomputing*, 363:246–260, 2019.
- [16] Xin Gu, Zhongjun Hou, and Jun Cai. Data-based flooding fault diagnosis of proton exchange membrane fuel cell systems using lstm networks. *Energy and AI*, 4:100056, 2021.
- [17] Youming Wang and Lin Cheng. A combination of residual and long-short-term memory networks for bearing fault diagnosis based on time-series model analysis. *Measurement Science and Technology*, 32(1):015904, 2020.
- [18] Oleksandr I Provotar, Yaroslav M Linder, and Maksym M Veres. Unsupervised anomaly detection in time series using lstm-based autoencoders. In *2019 IEEE International Conference on Advanced Trends in Information Theory (ATIT)*, pages 513–517. IEEE, 2019.
- [19] Jinhao Lei, Chao Liu, and Dongxiang Jiang. Fault diagnosis of wind turbine based on long short-term memory networks. *Renewable energy*, 133:422–432, 2019.
- [20] Qingqing Zhang, Jiyang Zhang, Jianxiao Zou, and Shicai Fan. A novel fault diagnosis method based on stacked lstm. *IFAC-PapersOnLine*, 53(2):790–795, 2020.
- [21] Kwangsuk Lee, Jae-Kyeong Kim, Jaehyong Kim, Kyeon Hur, and Hagbae Kim. Cnn and gru combination scheme for bearing anomaly detection in rotating machinery health monitoring. In *2018 1st IEEE International conference on knowledge innovation and invention (ICKII)*, pages 102–105. IEEE, 2018.
- [22] Fan Zhang, Qunying Liu, Yilu Liu, Ning Tong, Shuheng Chen, and Changhua Zhang. Novel fault location method for power systems based on attention mechanism and double structure gru neural network. *IEEE Access*, 8:75237–75248, 2020.
- [23] XuTing Mao, Feng Zhang, Gang Wang, Yan Chu, and KaiFu Yuan. Semi-random subspace with bi-gru: Fusing statistical and deep representation features for bearing fault diagnosis. *Measurement*, 173:108603, 2021.
- [24] Gao Yue, Gong Ping, and Li Lanxin. An end-to-end model based on cnn-lstm for industrial fault diagnosis and prognosis. In *2018 international conference on network infrastructure and digital content (IC-NIDC)*, pages 274–278. IEEE, 2018.
- [25] Levent Eren, Turker Ince, and Serkan Kiranyaz. A generic intelligent bearing fault diagnosis system using compact adaptive 1d cnn classifier. *Journal of Signal Processing Systems*, 91(2):179–189, 2019.
- [26] Xiaohan Chen, Beike Zhang, and Dong Gao. Bearing fault diagnosis base on multi-scale cnn and lstm model. *Journal of Intelligent Manufacturing*, 32:971–987, 2021.
- [27] Jiyang Zhang, Yuxuan Wang, Jianxiong Tang, Jianxiao Zou, and Shicai Fan. Ms-tcn: A multiscale temporal convolutional network for fault diagnosis in industrial processes. In *2021 American Control Conference (ACC)*, pages 1601–1606. IEEE, 2021.
- [28] Hanxiao Liu, Zihang Dai, David R So, and Quoc V Le. Pay attention to mlps. *arXiv preprint arXiv:2105.08050*, 2021.
- [29] Ilya Tolstikhin, Neil Houlsby, Alexander Kolesnikov, Lucas Beyer, Xiaohua Zhai, Thomas Unterthiner, Jessica Yung, Daniel Keysers, Jakob Uszkoreit, Mario Lucic, et al. Mlp-mixer: An all-mlp architecture for vision. *arXiv preprint arXiv:2105.01601*, 2021.
- [30] James Lee-Thorp, Joshua Ainslie, Ilya Eckstein, and Santiago Ontanon. Fnet: Mixing tokens with fourier transforms. *arXiv preprint arXiv:2105.03824*, 2021.
- [31] Peter M Atkinson and Adrian RL Tatnall. Introduction neural networks in remote sensing. *International Journal of remote sensing*, 18(4):699–709, 1997.
- [32] Fabio Pacifici, Marco Chini, and William J Emery. A neural network approach using multi-scale textural metrics from very high-resolution panchromatic imagery for urban land-use classification. *Remote Sensing of Environment*, 113(6):1276–1292, 2009.
- [33] Sergey Ioffe and Christian Szegedy. Batch normalization: Accelerating deep network training by reducing internal covariate shift. In *International conference on machine learning*, pages 448–456. PMLR, 2015.
- [34] Ashish Vaswani, Noam Shazeer, Niki Parmar, Jakob Uszkoreit, Llion Jones, Aidan N Gomez, Łukasz Kaiser, and Illia Polosukhin. Attention is all you need. In *Advances in neural information processing systems*, pages 5998–6008, 2017.
- [35] James J Downs and Ernest F Vogel. A plant-wide industrial process control problem. *Computers & chemical engineering*, 17(3):245–255, 1993.
- [36] Richard Lippmann, Joshua W Haines, David J Fried, Jonathan Korba, and Kumar Das. The 1999 darpa off-line intrusion detection evaluation. *Computer networks*, 34(4):579–595, 2000.